Surface superconductivity in a three-dimensional Cd_3As_2 semimetal at the interface with a gold contact

O. O. Shvetsov,[1,2] V. D. Esin,[1] A. V. Timonina,[1] N. N. Kolesnikov,[1] and E. V. Deviatov[1]

[1]*Institute of Solid State Physics of the Russian Academy of Sciences, Chernogolovka, Moscow District, 2 Academician Ossipyan str., 142432 Russia*

[2]*Moscow Institute of Physics and Technology, Institutsky lane 9, Dolgoprudny, Moscow region, 141700 Russia*

(Received 6 November 2018; revised manuscript received 19 March 2019; published 29 March 2019)

We experimentally investigate charge transport through a single planar junction between a Cd_3As_2 Dirac semimetal and a normal Au lead. For nonsuperconducting bulk Cd_3As_2 samples we observe non-Ohmic $dV/dI(V)$ curves, which strongly resemble standard Andreev reflection with a well-defined superconducting gap. Andreev-like behavior is demonstrated for Cd_3As_2 samples with different surface and contact preparation techniques. We connect this behavior with surface superconductivity due to the flat-band formation in Cd_3As_2, which has been predicted theoretically. The conclusion on superconductivity is also supported by the gap suppression by magnetic fields or temperature.

DOI: 10.1103/PhysRevB.99.125305

I. INTRODUCTION

Cd_3As_2 is predicted to be a three-dimensional Dirac semimetal [1], so it has symmetry-protected conic dispersion in the bulk spectrum [2,3], which has been experimentally confirmed by angle-resolved photoemission spectroscopy (ARPES) [4,5] and scanning tunneling microscopy [6] measurements. Due to the Dirac spectrum, Cd_3As_2 demonstrates interesting physical properties, e.g., unusual magnetoresistance phenomena, associated with chiral anomaly [7,8], and ultrahigh carrier mobility [9,10]. Some features of exotic surface transport have been demonstrated by observation of quantum oscillations [11].

By breaking certain symmetries, Cd_3As_2 can be driven to different topological phases [2], such as topological insulator [12], Weyl semimetal [13,14], or even topological superconductor [15–17]. The latter is notably attractive due to the surface states hosting Majorana fermions [16,18–20].

There are two ways to induce superconductivity in bulk Cd_3As_2: by carrier doping [2], which is only a theoretical prediction so far, or by external pressure [21]. In the latter case bulk superconductivity appears [21] around 3.5 GPa. In addition, point contact spectroscopy experiments [22,23] reveal signatures of superconductivity in a tip contact region (so-called tip induced superconductivity), while no effect is observed in the case of a soft contact [23]. The origin of the effect is still debatable, e.g., it is not clear whether pressure of a tip is enough to induce superconductivity in Cd_3As_2.

On the other hand, flat-band formation stimulates surface superconductivity [24–27]. In the presence of attractive interaction due to electron-phonon coupling [21], the high density of states associated with these flat bands dramatically increases the superconducting transition temperature. This property is generic and does not depend much on the details of the system [25]. In particular, superconductivity has been observed in twisted bilayer graphene [28–30].

Flat bands may emerge due to interaction [31,32] or topological effects [25,33–35]. Historically flat bands were first discussed in the context of Landau levels. Now they are considered as a class of fermionic systems with a dispersionless spectrum that has exactly zero energy, i.e., with diverging density of states. Interaction effects could be expected for high-mobility carriers [1] in Cd_3As_2. The simplest example of topological flat-band formation is known for nodal-line semimetals [33,34]. On the boundary of each topological insulator inside the nodal loop there should be the zero energy state. But this occurs for all the insulators inside the loop, so all these zero energy states on the surface form the two-dimensional (2D) flat band. The topological flat-band formation is not also impossible for Cd_3As_2 material, since it is known to experience transition to different topological phases [2,36,37]. It is important that if surface superconductivity appears in a Cd_3As_2 Dirac semimetal due to fundamental effects, it should be independent on the contact preparation technique.

Here we experimentally investigate charge transport through a single planar junction between a Cd_3As_2 Dirac semimetal and a normal Au lead. For nonsuperconducting bulk Cd_3As_2 samples we observe non-Ohmic $dV/dI(V)$ curves, which strongly resemble standard Andreev reflection with a well-defined superconducting gap. Andreev-like behavior is demonstrated for Cd_3As_2 samples with different surface and contact preparation techniques. We connect this behavior with surface superconductivity due to the flat-band formation in Cd_3As_2, which has been predicted theoretically. The conclusion on superconductivity is also supported by the gap suppression by magnetic field or temperature.

II. SAMPLES AND TECHNIQUE

Cd_3As_2 crystals were grown by crystallization of molten drops in the convective counterflow of argon held at 5 MPa pressure. For the source of the drops the stalagmometer similar to one described [38] was applied. The crystals sometimes had signs of partial habit of α-Cd_3As_2 tetragonal structure.

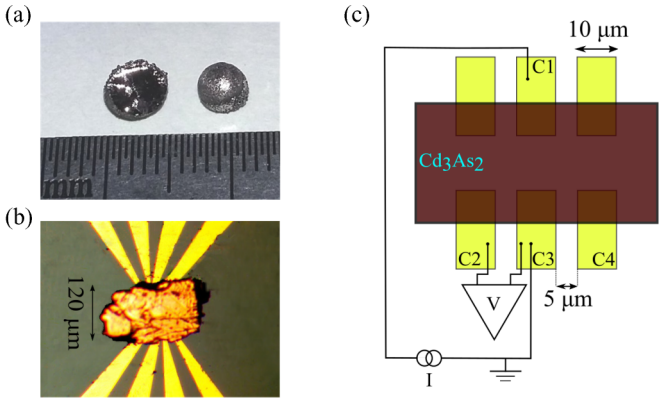

FIG. 1. (a) An initial Cd_3As_2 drop (right) and one cleaved along (112) (left). (b) Top-view image of the sample with a small Cd_3As_2 single crystal. (c) The sketch of a sample with electrical connections. 100 nm thick and 10 μm wide Au leads are formed on a SiO_2 substrate. A Cd_3As_2 single crystal ($\approx$100 μm size) is transferred on top of the leads with $\approx$10 μm overlap, forming planar junctions. Charge transport is investigated with a standard three-point technique: the studied contact (C3) is grounded and two other contacts (C1 and C2) are used for applying current and measuring potential.

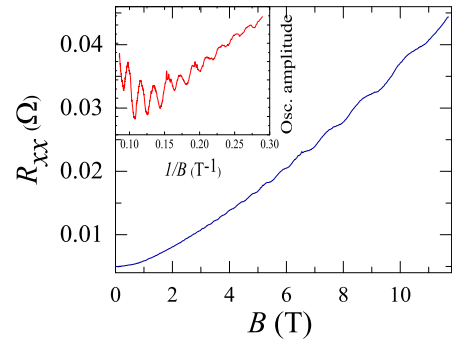

FIG. 2. Transverse four-point magnetoresistance with Shubnikov–de Haas oscillations in high magnetic fields [1] for one of our samples at 60 mK. The ac measurement current is 2.5 μA at 110 Hz, the ac xx voltage is measured by lock-in after a preamplifier. Inset demonstrates perfect periodicity of the oscillations in the inverse magnetic field. The data in the inset are obtained by subtracting a linear dependence from the raw $R(B)$ curve, shown in the main figure.

About one fifth of the drops were single crystals, like ones depicted in Fig. 1(a). The EDX measurements and x-ray powder diffractograms always confirmed pure Cd_3As_2.

Figure 1(b) shows a top-view image of a sample. The leads pattern is formed by lift-off technique after thermal evaporation of 100 nm Au on the insulating SiO_2 substrate. The 10 μm wide Au leads are separated by 5 μm intervals, see Fig. 1(b).

Small (less than 100 μm size) Cd_3As_2 single crystals are obtained by a mechanical cleaving method, somewhat similar to that described in Ref. [39]: we crush the initial 5 mm size Cd_3As_2 single crystal into small fragments. This procedure allows us to create a clean Cd_3As_2 surface without mechanical polishing or chemical treatment.

Then, the obtained small Cd_3As_2 crystal is transferred to the Au leads pattern and pressed slightly with another oxidized silicon substrate. A special metallic frame allows us to keep the substrates parallel and apply a weak pressure to the piece. No external pressure is needed for a Cd_3As_2 crystal to hold on to a substrate with Au leads afterward.

For comparison, we also defined 100×100 μm^2 Au contacts by standard photolithography on the cleaved along (112) and mechanically polished surface of the initial Cd_3As_2 drop. In this case, Cd_3As_2 surface degradation could be expected due to the polishing process [40].

We check by standard magnetoresistance measurements that our Cd_3As_2 samples demonstrate large magnetoresistance with Shubnikov–de Haas oscillations in high magnetic fields [1], see Fig. 2, indicating high quality of Cd_3As_2. From the oscillations' period in the inverse magnetic field, see the inset, and zero-field resistance value we estimate the concentration of carries as $n \approx 2.3 \times 10^{18}$ cm^{-3} and low-temperature mobility as $\mu \approx 10^6$ cm^2/V s, which is in good correspondence with known values [1].

We study electron transport across a single Au-Cd_3As_2 junction in a standard three-point technique, see Fig. 1(a): one Au contact is grounded and two other contacts are used for applying current and measuring Cd_3As_2 potential. To obtain $dV/dI(V)$ characteristics, dc current is additionally modulated by a low (below the dc points step) ac component. We measure both dc (V) and ac ($\sim dV/dI$) components of the potential with a dc voltmeter and a lock-in, respectively. We check that the lock-in signal is independent of the modulation frequency. The measurements are performed in a dilution refrigerator equipped with a superconducting solenoid.

III. EXPERIMENTAL RESULTS

Examples of $dV/dI(V)$ characteristics are shown in Fig. 3 for different Au-Cd_3As_2 junctions. Since the $dV/dI(V)$ curves of the junctions might be sensitive to the interface quality, e.g., as it is known for normal-superconductor junctions [41], Figs. 3(a) and 3(c) demonstrate maximum device-to-device fluctuations for samples with cleaved Cd_3As_2 fragments, while Fig. 3(d) shows the $dV/dI(V)$ curve variation for large junctions on a polished Cd_3As_2 surface.

The main experimental finding is the prominent non-Ohmic behavior, which is reflected in an about 10% resistance dip around zero bias. This behavior is well reproducible for different samples, see Fig. 3: while the shape and the width of the dip may vary from sample to sample, the qualitative behavior is the same.

$dV/dI(V)$ characteristics are shown in Fig. 3(a) for two different positions of a voltage probe for the same Au-Cd_3As_2 junction. In the three-point configuration, the measured potential reflects the in-series connected resistances of the grounded Au lead, the Au-Cd_3As_2 interface, and the bulk resistance of Cd_3As_2. If one changes only the voltage probe position, two former contributions are invariant. Only the contribution of the bulk Cd_3As_2 resistance is varied, which we detect as the resistance level change δR in Fig. 3(a). The curves coincide with high accuracy after subtracting δR and $I\delta R$ from dV/dI and V components of the upper curve, see Fig. 3(b), so the dV/dI dip does not originate from the Cd_3As_2 bulk. We

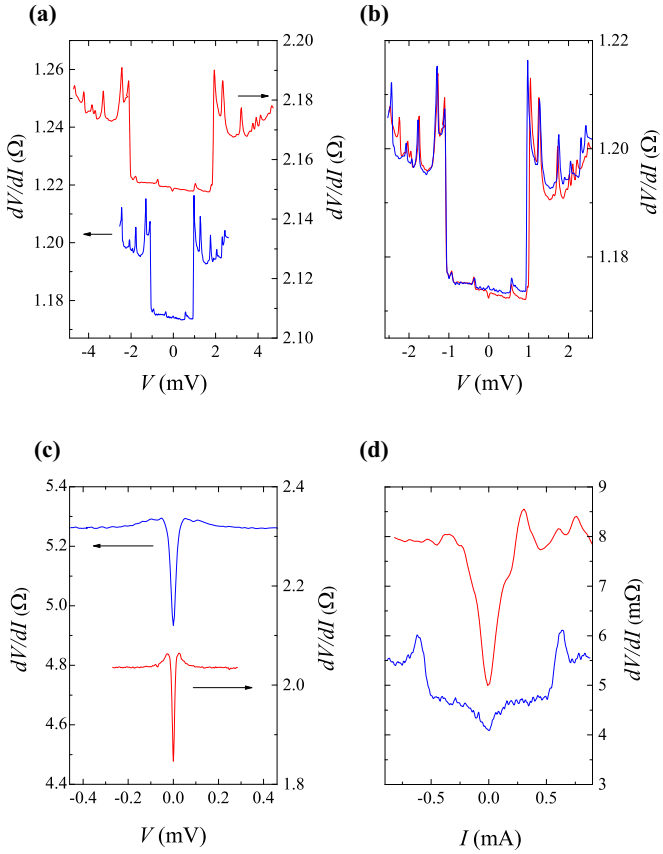

FIG. 3. Examples of $dV/dI(V)$ characteristics are shown for different Au-Cd_3As_2 junctions. The main experimental finding is the prominent non-Ohmic behavior, which is reflected as an about 10% resistance dip around zero bias and is well reproducible for different samples. (a) $dV/dI(V)$ characteristics for the same Au-Cd_3As_2 junction, obtained for two different voltage probes, which allows us to estimate the bulk resistance contribution. (b) Coincidence of the curves from (a) after subtracting the bulk resistance (see the text). Comparison of (a) and (c) demonstrates maximum device-to-device fluctuations for junctions with cleaved Cd_3As_2 fragments, while (d) shows the $dV/dI(V)$ curve variation for polished Au-Cd_3As_2 junctions. The curves are obtained at 60 mK in zero magnetic field.

should relate the resistance dip with the Au-Cd_3As_2 interface contribution, since non-Ohmic $dV/dI(V)$ behavior cannot be linked with the Au lead.

It is clear that $dV/dI(V)$ characteristics of the Au-Cd_3As_2 interface strongly resemble standard Andreev reflection behavior [42,43] for transparent normal-superconducting junctions. This conclusion is supported by $dV/dI(V)$ nonlinearity suppression by magnetic field or temperature: despite the different shape of the original $dV/dI(V)$ curves in Fig. 3, all of them become flat above some critical temperature or magnetic field.

We give an example of temperature and magnetic field evolution in Figs. 4 and 5 for the junction from Fig. 3(a). The width of the dV/dI dip is gradually diminishing, as it is shown in Fig. 4(b) and in the inset to Fig. 5 as a function of temperature and magnetic field, respectively. The behavior strongly resembles the known one [43] for a superconducting gap, but the data cannot be fitted by standard

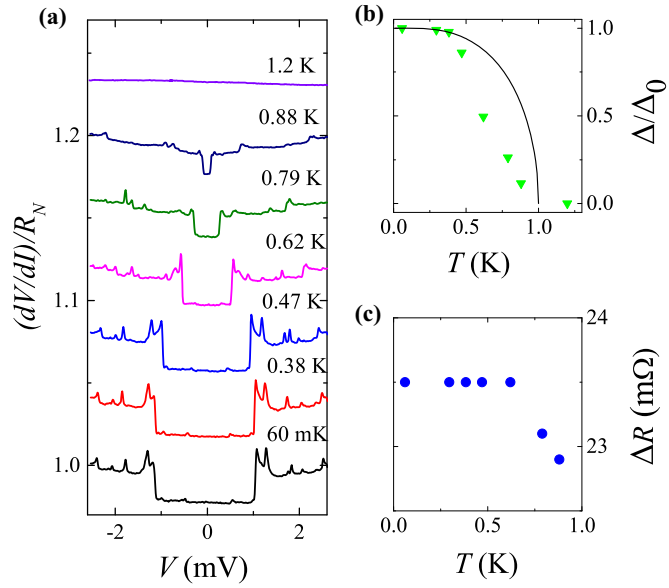

FIG. 4. (a) Suppression of $dV/dI(V)$ nonlinearity by temperature. The curves are shifted for clarity. (b) The gap Δ obtained as the nonlinearity width at half of its maximum depth, as a function of temperature. The data resemble superconducting gap behavior, but they cannot be fitted by standard BCS dependence [43] (black line). (c) The depth ΔR of the resistance dip at zero bias, which is consistent with the BTK dependence [41,43] for the transparent interface. The data are shown for zero magnetic field.

BCS temperature dependence, and $(1 - H^2/H_c^2)$ magnetic field law [the solid lines in Fig. 4(b) and in the inset to Fig. 5], known for the conventional superconductors [43]. Thus, the unconventional superconductivity is possible, like it was

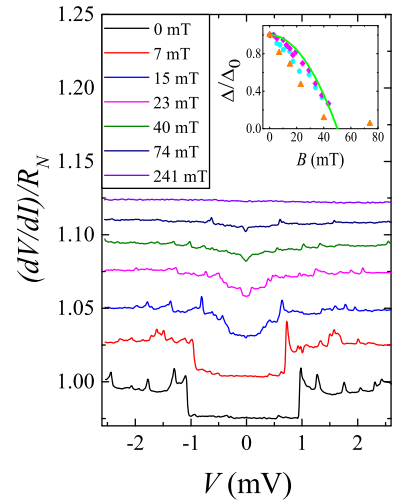

FIG. 5. Suppression of $dV/dI(V)$ nonlinearity by normal magnetic field at 60 mK temperature. The curves are shifted for clarity. Inset demonstrates the gap Δ (triangles), obtained as the nonlinearity width at half of its maximum depth, diminishing with magnetic field, as also expected for the superconducting gap. The data cannot be well fitted by standard dependence [43] (green line), which may hint to the unconventional superconductivity [22,23]. The gap weakly depends on the field orientation, as it is shown for another sample by circles (in-plane field orientation) and diamonds (normal one).

proposed in point contact spectroscopy experiments [22,23]. The critical temperature can be estimated as $T_c \approx 1$ K in the inset to Fig. 4 [note that the curves in Figs. 3(a) and 3(b) still contain an unknown bulk contribution]. For the samples in Figs. 3(c) and 3(d) we estimate T_c as 300 mK and 1 K, B_c as 26 and 140 mT, respectively.

The bulk Cd_3As_2 material is not superconducting [21], which is confirmed by finite four-point resistance in Fig. 2. Since an Au lead is also normal, the Andreev-like behavior of experimental $dV/dI(V)$ curves should reflect surface superconductivity at the Au-Cd_3As_2 interface.

IV. DISCUSSION

As a result, we observe $dV/dI(V)$ curves, which are qualitatively analogous to tip induced superconductivity [22,23], for wide planar contacts without external pressure.

Formally, standard BTK theory [41] is appropriate in the ballistic limit, when the contact diameter is less than elastic and inelastic mean free paths. In the opposite (thermal) limit, peaks in dV/dI reflect superconducting transition due to the critical current in the junction.

The ballistic regime is obviously realized for the clean Cd_3As_2 surface, as we see in Figs. 3(a) and 3(b), since the mean free path exceeds 25 μm at a given concentration and mobility. In this case, in contrast to the tip experiments, the width of the dip is defined by the superconducting gap for the best junctions, like in Fig. 3(a), as it is expected [41–43] for standard Andreev reflection [44,45]. This conclusion is supported by qualitative behavior of $\Delta(T)$ and $\Delta(B)$ dependencies in Fig. 4(b) and in the inset to Fig. 5. Also, the depth ΔR of the resistance dip is nearly constant at low temperatures, see Fig. 4(c), which is consistent with the BTK dependence [41,43] for the transparent interface. We wish to emphasize here that the actual gap value is smaller than the width of the dip in Figs. 4 and 5 because the $dV/dI(V)$ curves in Figs. 3(a) and 3(b) still contain an unknown bulk contribution. The actual gap value should be obtained from the $\Delta(T)$ dependence.

The thermal limit is obviously realized for the polished Cd_3As_2 surface with large contacts in Fig. 3(d), so the differential resistance is driven by current, which achieves the critical value I_c at low (about 1 μV) imbalances at the interface. We wish to mention that for narrow superconductors between two massive normal metals, electron cotunneling and crossed Andreev reflection should be taken into account [46]. Both these effects are extremely sensitive to the transmission of the interfaces, see Fig. 12 in Ref. [46], which should be responsible for the device-to-device fluctuations in Figs. 3(a) and 3(c).

The interface superconductivity has been demonstrated in a number of various systems, with different discussed microscopic mechanisms [47]. In our experiment, superconductivity should originate from fundamental effects in a topological Dirac semimetal, since it is independent of contact preparation details. The obvious candidate is the flat-band formation [24–27] due to interaction or topology. For our samples with the bulk carrier density $n \approx 2.3 \times 10^{18}$ cm^{-3} and the corresponding [1] effective mass 0.044, the interaction parameter r_s is about 1. Even if this value is enhanced for low densities near the sample surface, it seems to be too small to produce noticeable interaction effects [31,32]. On the other hand, the Cd_3As_2 Dirac semimetal is known to experience transition to different topological phases [2], so one could propose a topological mechanism, similar to surface states in nodal-line semimetals [25,33–35]. The possibility of such transitions is also supported by recent theoretical predictions for different semimetal systems [36]. For the Cd_3As_2 Dirac semimetal, flat bands are evidenced in ARPES [48,49] and magneto-optics [50,51] experiments.

Another possibility is the strain effects. In Dirac semimetals strain generically acts as an effective gauge field on Dirac fermions and creates pseudo-Landau orbitals without breaking time-reversal symmetry [37]. The zero-energy Landau orbitals form a flat band in the vicinity of the Dirac point, so the high density of states of this flat band gives rise to interface superconductivity. We observe finite four-point resistance between different contacts in Fig. 2, which well correspond to the fact that strain-induced flat-band formation only occurs at the Au-Cd_3As_2 interface due to materials misfit.

V. CONCLUSION

As a conclusion we experimentally investigate charge transport through a single planar junction between a Cd_3As_2 Dirac semimetal and a normal Au lead. For nonsuperconducting bulk Cd_3As_2 samples, we observe non-Ohmic $dV/dI(V)$ curves, which strongly resemble standard Andreev reflection with a well-defined superconducting gap. Andreev-like behavior is demonstrated for Cd_3As_2 samples with different surface and contact preparation techniques. We connect this behavior with surface superconductivity due to the flat-band formation in Cd_3As_2, which has been predicted theoretically. The conclusion on superconductivity is also supported by the gap suppression by magnetic fields or temperature.

ACKNOWLEDGMENTS

We wish to thank A. Kononov for help with the experimental setup, and G. E. Volovik, Yu. S. Barash, and V. T. Dolgopolov for fruitful discussions. We gratefully acknowledge financial support partially by the RFBR (Project No. 19-02-00203), RAS, and RF State task.

[1] For a review on Cd_3As_2 properties, see I. Crassee, R. Sankar, W.-L. Lee, A. Akrap, and M. Orlita, Phys. Rev. Mater. **2**, 120302 (2018).

[2] Z. Wang, H. Weng, Q. Wu, X. Dai, and Z. Fang, Phys. Rev. B **88**, 125427 (2013).

[3] Z. Wang, Y. Sun, X.-Q. Chen, C. Franchini, G. Xu, H. Weng, X. Dai, and Z. Fang, Phys. Rev. B **85**, 195320 (2012).

[4] Z. K. Liu, J. Jiang, B. Zhou, Z. J. Wang, Y. Zhang, H. M. Weng, D. Prabhakaran, S. K. Mo, H. Peng, P. Dudin, T. Kim,

M. Hoesch, Z. Fang, X. Dai, Z. X. Shen, D. L. Feng, Z. Hussain, and Y. L. Chen, Nat. Mater. **13**, 677 (2014).
[5] S. Borisenko, Q. Gibson, D. Evtushinsky, V. Zabolotnyy, B. Büchner, and R. J. Cava, Phys. Rev. Lett. **113**, 027603 (2014).
[6] S. Jeon, B. B. Zhou, A. Gyenis, B. E. Feldman, I. Kimchi, A. C. Potter, Q. D. Gibson, R. J. Cava, A. Vishwanath, and A. Yazdani, Nat. Mater. **13**, 851 (2014).
[7] H. Li, H.-W. Wang, H. He, J. Wang, and S.-Q. Shen, Phys. Rev. B **97**, 201110(R) (2018).
[8] M. Wu, G. Zheng, W. Chu, Y. Liu, W. Gao, H. Zhang, J. Lu, Y. Han, J. Zhou, W. Ning, and M. Tian, Phys. Rev. B **98**, 161110(R) (2018).
[9] T. Liang, Q. Gibson, M. N. Ali, M. Liu, R. J. Cava, and N. P. Ong, Nat. Mater. **14**, 280 (2014).
[10] W. J. Turner, A. S. Fischler, and W. E. Reese, Phys. Rev. **121**, 759 (1961).
[11] G. Zheng, M. Wu, H. Zhang, W. Chu, W. Gao, J. Lu, Y. Han, J. Yang, H. Du, W. Ning, Y. Zhang, and M. Tian, Phys. Rev. B **96**, 121407(R) (2017).
[12] M. Z. Hasan and C. L. Kane, Rev. Mod. Phys. **82**, 3045 (2010).
[13] A. A. Burkov and L. Balents, Phys. Rev. Lett. **107**, 127205 (2011).
[14] X. Wan, A. M. Turner, A. Vishwanath, and S. Y. Savrasov, Phys. Rev. B **83**, 205101 (2011).
[15] X.-L. Qi and S.-C. Zhang, Rev. Mod. Phys. **83**, 1057 (2011).
[16] L. Fu and C. L. Kane, Phys. Rev. Lett. **100**, 096407 (2008).
[17] X.-L. Qi, T. L. Hughes, and S.-C. Zhang, Phys. Rev. B **81**, 134508 (2010).
[18] N. Read and D. Green, Phys. Rev. B **61**, 10267 (2000).
[19] A. Y. Kitaev, Phys. Usp. **44**, 131 (2001).
[20] D. A. Ivanov, Phys. Rev. Lett. **86**, 268 (2001).
[21] L. He, Y. Jia, S. Zhang, X. Hong, C. Jin, and S. Li, Npj Quantum Mater. **1**, 16014 (2016).
[22] L. Aggarwal, A. Gaurav, G. S. Thakur, Z. Haque, A. K. Ganguli, and G. Sheet, Nat. Mater. **15**, 32 (2016).
[23] H. Wang, H. Wang, H. Liu, H. Lu, W. Yang, S. Jia, X.-J. Liu, X. C. Xie, J. Wei, and J. Wang, Nat. Mater. **15**, 38 (2016).
[24] Yu. S. Barash and P. I. Nagornykh, JETP Lett. **83**, 376 (2006).
[25] N. B. Kopnin, T. T. Heikkilä, and G. E. Volovik, Phys. Rev. B **83**, 220503(R) (2011).
[26] T. T. Heikkilä and G. E. Volovik, Springer Ser. Mater. Sci. **244**, 123 (2016).
[27] L. Liang, T. I. Vanhala, S. Peotta, T. Siro, A. Harju, and P. Törmä, Phys. Rev. B **95**, 024515 (2017).
[28] Y. Cao, V. Fatemi, S. Fang, K. Watanabe, T. Taniguchi, E. Kaxiras, and P. Jarillo-Herrero, Nature (London) **556**, 43 (2018).
[29] Y. Cao, V. Fatemi, A. Demir, S. Fang, S. L. Tomarken, J. Y. Luo, J. D. Sanchez-Yamagishi, K. Watanabe, T. Taniguchi, E. Kaxiras, R. C. Ashoori, and P. Jarillo-Herrero, Nature (London) **556**, 80 (2018).
[30] M. Yankowitz, S. Chen, H. Polshyn, K. Watanabe, T. Taniguchi, D. Graf, A. F. Young, and C. R. Dean, Science **363**, 1059 (2019).
[31] D. Yudin, D. Hirschmeier, H. Hafermann, O. Eriksson, A. I. Lichtenstein, and M. I. Katsnelson, Phys. Rev. Lett. **112**, 070403 (2014).
[32] G. E. Volovik, JETP Lett. **59**, 830 (1994).
[33] T. T. Heikkilä and G. E. Volovik, JETP Lett. **93**, 59 (2011).
[34] T. T. Heikkilä, N. B. Kopnin, and G. E. Volovik, JETP Lett. **94**, 233 (2011).
[35] G. P. Mikitik and Yu. V. Sharlai, Phys. Rev. B **90**, 155122 (2014).
[36] Z. Liu, H. Xin, L. Fu, Y. Liu, T. Song, X. Cui, G. Zhao, and J. Zhao, J. Phys. Chem. Lett. **10**, 244 (2019).
[37] E. Tang and L. Fu, Nat. Phys. **10**, 964 (2014).
[38] N. N. Kolesnikov, M. P. Kulakov, Yu. N. Ivanov, J. Cryst. Growth **125**, 576 (1992).
[39] W. Yu, W. Pan, D. L. Medlin, M. A. Rodriguez, S. R. Lee, Zhi-qiang Bao, and F. Zhang, Phys. Rev. Lett. **120**, 177704 (2018).
[40] I. Crassee, E. Martino, C. C. Homes, O. Caha, J. Novák, P. Tückmantel, M. Hakl, A. Nateprov, E. Arushanov, Q. D. Gibson, R. J. Cava, S. M. Koohpayeh, K. E. Arpino, T. M. McQueen, M. Orlita, and A. Akrap, Phys. Rev. B **97**, 125204 (2018).
[41] G. E. Blonder, M. Tinkham, and T. M. Klapwijk, Phys. Rev. B **25**, 4515 (1982).
[42] A. F. Andreev, Sov. Phys. JETP **19**, 1228 (1964).
[43] M. Tinkham, *Introduction to Superconductivity*, 2nd ed. (McGraw-Hill, New York, 1996).
[44] A. Kononov, V. A. Kostarev, B. R. Semyagin, V. V. Preobrazhenskii, M. A. Putyato, E. A. Emelyanov, and E. V. Deviatov, Phys. Rev. B **96**, 245304 (2017).
[45] A. Kononov, S. V. Egorov, Z. D. Kvon, N. N. Mikhailov, S. A. Dvoretsky, and E. V. Deviatov, Phys. Rev. B **93**, 041303(R) (2016).
[46] R. Melin, F. S. Bergeret, and A. Levy Yeyati, Phys. Rev. B **79**, 104518 (2009).
[47] For a review, see Y. Saito, T. Nojima and Y. Iwasa, Nat. Rev. Mater. **2**, 16094 (2016).
[48] M. Neupane, S.-Y. Xu, R. Sankar, N. Alidoust, G. Bian, C. Liu, I. Belopolski, T.-R. Chang, H.-T. Jeng, H. Lin, A. Bansil, F. Chou, and M. Zahid Hasan, Nat. Commun. **5**, 3786 (2014),
[49] S. Roth, H. Lee, A. Sterzi, M. Zacchigna, A. Politano, R. Sankar, F. C. Chou, G. Di Santo, L. Petaccia, O. V. Yazyev, and A. Crepaldi, Phys. Rev. B **97**, 165439 (2018).
[50] M. Hakl, S. Tchoumakov, I. Crassee, A. Akrap, B. A. Piot, C. Faugeras, G. Martinez, A. Nateprov, E. Arushanov, F. Teppe, R. Sankar, W.-l. Lee, J. Debray, O. Caha, J. Novák, M. O. Goerbig, M. Potemski, and M. Orlita, Phys. Rev. B **97**, 115206 (2018).
[51] A. Akrap, M. Hakl, S. Tchoumakov, I. Crassee, J. Kuba, M. O. Goerbig, C. C. Homes, O. Caha, J. Novák, F. Teppe, W. Desrat, S. Koohpayeh, L. Wu, N. P. Armitage, A. Nateprov, E. Arushanov, Q. D. Gibson, R. J. Cava, D. van der Marel, B. A. Piot, C. Faugeras, G. Martinez, M. Potemski, and M. Orlita, Phys. Rev. Lett. **117**, 136401 (2016).